Supplementary Information

Diversities of chromite mineralization induced by chemo-thermal variations of mantle during subduction initiation

Peng-Fei Zhang[1]*, Mei-Fu Zhou[1]*, Paul T. Robinson[1], John Malpas[2], Graciano P.Yumul Jr.[3], Christina Yan Wang[4], Jie Li[5]

1. State Key Laboratory of Geological Processes and Mineral Resources, China University of Geosciences, Wuhan, China
2. Department of Earth Sciences, The University of Hong Kong, Hong Kong, China
3. Cordillera Exploration Company, Inc., NAC Tower, BGC, Taguig City, Philippines
4. CAS Key Laboratory of Mineralogy and Metallogeny, Guangzhou Institute of Geochemistry, Chinese Academy of Sciences, Guangzhou, China
5. State Key Laboratory of Isotope Geochemistry, Guangzhou Institute of Geochemistry, Chinese Academy of Sciences, Guangzhou, China

* Corresponding author 1: Peng-Fei Zhang, zhangpengfei073061@163.com

* Corresponding author 2: Mei-Fu Zhou, zhoumeifu@hotmail.com

Supplementary Information List:

Supplementary Information to the Fig-1.

Papers cited for each ophiolitic block in the Fig.1 can be found as below and in the Supplementary References：

Sangun, Matsumoto et al. show[1]; ***Tari-Misaka***, Arai & Yurimoto show[2]; ***Sartohay***, Zhou et al. show[3]; ***Hegenshan***, Robinson et al. show[4]; ***Moa-Baracoa***, Proenza et al. show[5], Marchesi et al. show[6], Rui et al. show[7]; ***Coto***, Zhang et al. show[8]; ***Cabangan***, Yumul & Dimalanta show[9]; ***Medellin***, Hernández-González1 et al. show[10]; ***Outokumpu***, Liipo et al. show[11]; ***Mayarí-Crystal***, Proenza et al. show[5], Marchesi et al. show[6]; ***Acoje***, Zhang et al. show[12]; ***Cyprus***, Greenbaum show[13], Batanova & Sobolev show[14]; ***Kop***, Zhang et al. show[15]; ***Lycian***, Uysal et al. show[16,17], Xu et al. show[18]; ***Fizh***, Takazawa et al. show[19], Rollinson et al. show[20]; ***Tiebaghi***, Moutte show[21], Ulrich et al. show[22]; ***Kempirsai***, Melcher et al. show[23], Savelieva et al. show[24]; ***Kraka***, Saveliev & Fedoseev show[25], Garuti et al. show[26]; ***Purang***, Gong et al. show[27], Xiong et al. show[28]; ***Dongbo***, Xiong et al. show[29]; ***Zedang-Luobusa***, Xiong et al. show[30], Zhang et al. show[31].

Supplementary Fig-1.

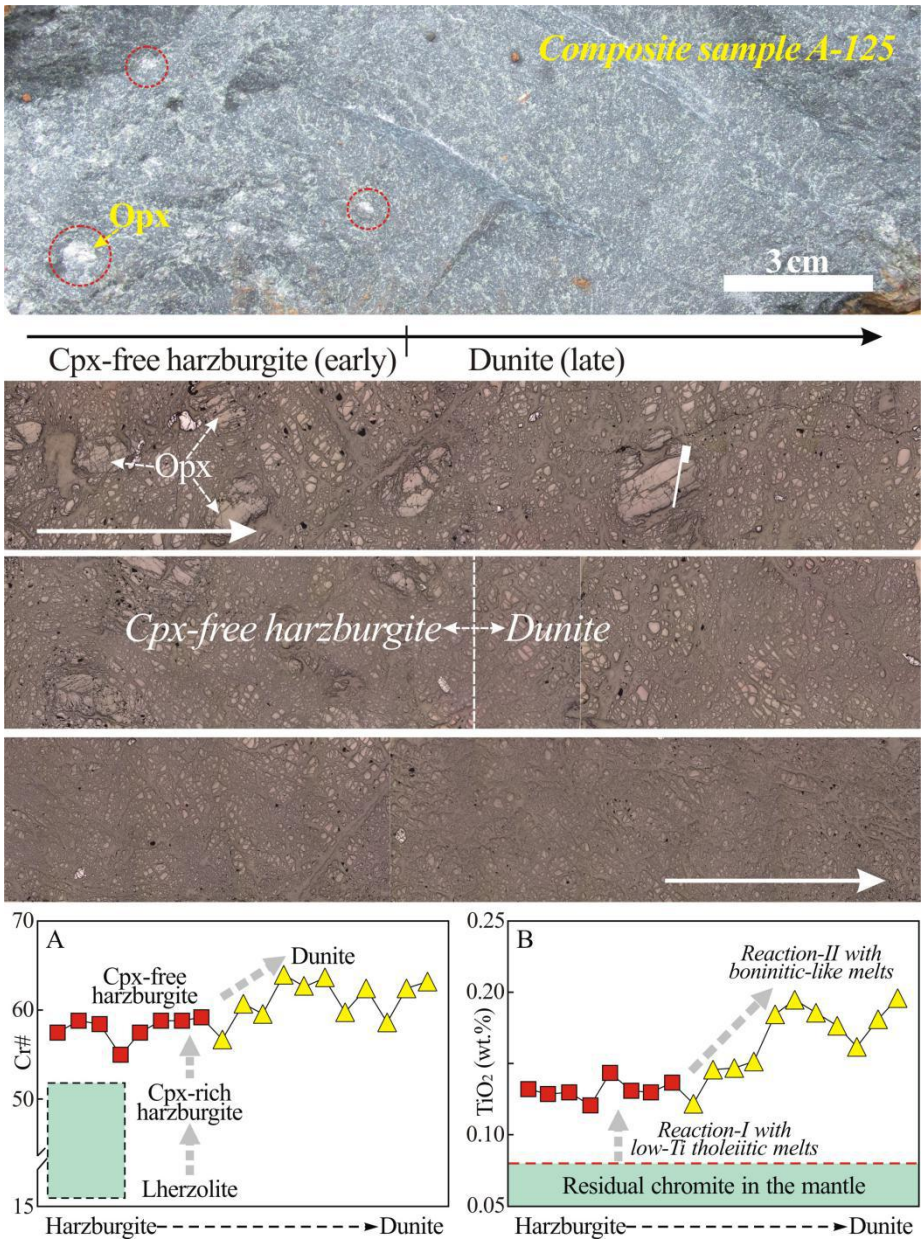

Supplementary Fig-1. Petrological and compositional variations in a composite sample of Cpx-free harzburgite and dunite from mantle sequence of the Acoje block. The hand-specimen and photo-micrographs above show decreasing modal% of orthopyroxene (Opx) from the Cpx-free harzburgite to the dunite parts, marked by the black and white arrows. (A): Variation of Cr# of chromite from the Cpx-free harzburgite to dunite. (B): Variation of TiO_2 contents of chromite from the Cpx-free harzburgite to dunite. Based on the Cr# and TiO_2 contents of chromite, the harzburgite part with high-Al chromite in the composite sample was not pure melting residue of FMM but had been modified by melt with low-Ti tholeiitic affinity (Reaction-I), whereas the dunite with high-Cr chromite was formed via reaction between Cpx-free harzburgite and boninitic-like melts (Reaction-II). The reactions elevated the TiO_2 contents of chromite twice from extremely low level of partial melting residue to ~ 0.2 wt.%. Such spatial relationship supports that low-Ti tholeiitic magmatism happened earlier than boninitic-like ones in the Acoje block, consistent with the framework of subduction initiation. The data of chromite are from Zhang et al. show[12].

Supplementary Fig-2.

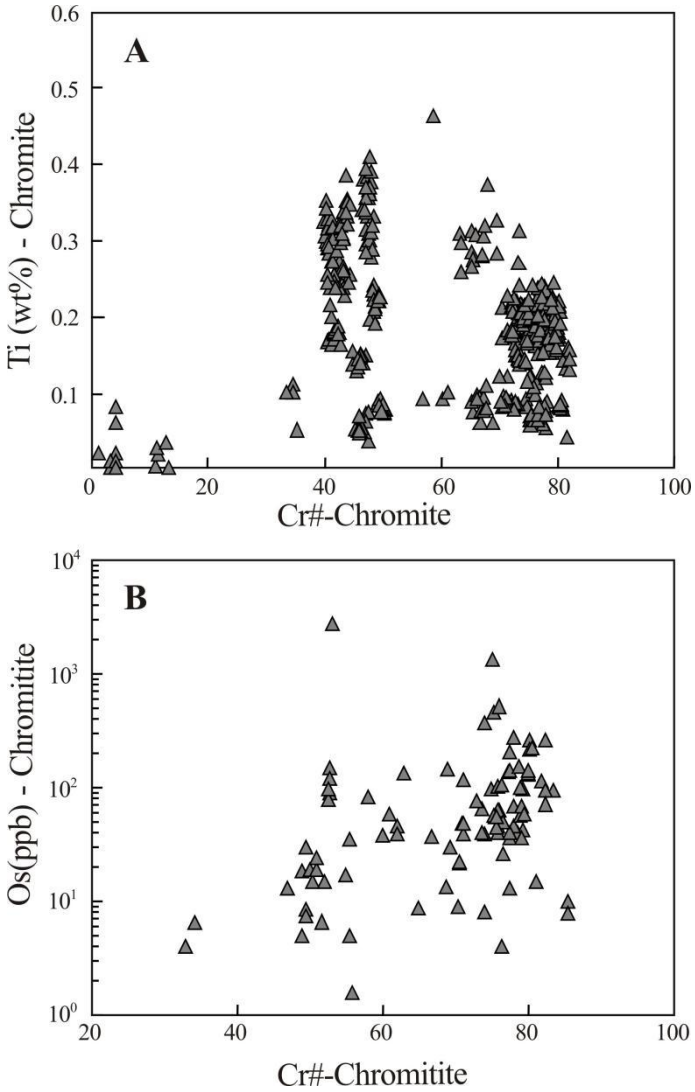

Supplementary Fig-2: Plots of TiO_2 vs. Cr# of chromite (A) and bulk-rock Os vs. Cr# of chromite (B) in ophiolitic chromitites worldwide. The data used in the panel A are from Zhang et al. Show[15], Xu et al. Show[18], Xiong et al. show[29,33], Zhou et al. show[32], Liu et al. show[34], and Su et al., show[35]. The data used in the panel B are from Uysal et al. show[16], Xiong et al. Show[28,29,37,38], and Gervilla et al. show[36].

Supplementary Note-1: Geological background of the Zambales ophiolite

The Zambales ophiolite, situated in northwest Luzon Island (Fig. 2A-B), ~ 130 km long and 4500 km^2 big in area[39]. The ophiolite consists from north to south of the Masinloc, Cabangan, and San Antonio massifs (Fig. 2B). The Masinloc massif is the biggest and further divided into the Acoje block in the north and the Coto block in the south[40,41] (Fig. 2B), which host world-class high-Cr and high-Al chromite deposits, respectively (25 Mt *vs* 6.34 Mt)[42]. Systematic chronological studies documented that the magmatism in the Acoje block took place later than in the Coto block (44-43 *vs* 45 Ma)[43,44], but the two blocks were revealed as adjacent parts of the same proto-forearc lithosphere with transitional compositions and generated in an evolving subduction initiation system[8,43,47]. The Coto block records the stage of proto-forearc spreading before boninitic magmatism, including an early stage of FAB magmatism and a later stage of arc tholeiitic magmatism, whereas the Acoje block exhibits magmatism varying from arc tholeiitic to boninitic types[43,45-48].

The Coto block contains four stratigraphic sequences: harzburgitic mantle, dunitic MTZ, mafic cumulates, and a volcanic-hypabyssal suite[40,43,48,49] (Supplementary Fig. 3A-B; Fig. 2C). The mantle sequence of the block is mainly made of Cpx-poor harzburgites with few clinopyroxene, and there is no obvious variation of mineral proportions is observed from top to bottom of the mantle sequence[8,40,49] (Fig. 3). There is no evidence suggesting that the mantle sequence of the block was ever refertilized either. Clinopyroxene and chromite in the harzburgites at different stratigraphic levels show limited chemical variations and have compositions similar to their counterparts in the Acoje Cpx-poor harzburgites[49] (Fig. 3). The MTZ is mainly made of serpentinized dunites and host chromitite pods near the mantle-MTZ border[8,50] (Fig. 2C and 3). Chromite in the ores share similar Cr#s to those high-Al ones in the Acoje block but have large TiO_2 variation (< 0.07-0.28%)[8,32] (Fig. 3 and 5). Geochemical studies suggest the Coto block successively experienced FAB and IAT magmatism in a proto-forearc setting[43,45]. However, development of the Coto block expired after the IAT magmatism and high-Al chromite mineralization, leaving no obvious record of boninitic magmatism in the block.

The Acoje block is also divided into four sequences from west to east: mantle, Moho Transition zone (MTZ), mafic cumulates and hypabyssal-volcanic rocks[45,52] (Fig. 2D). The uppermost part of the mantle sequence mainly comprises of Cpx-poor harzburgites that contain dunite and Cpx-rich harzburgite bodies[12,40,49,51] (Fig. 2D and 3). From top to bottom of the mantle sequence, there is an increasing trend of pyroxene modal%, which can be judged from the pyroxene relicts on the weathered surfaces of peridotites (Supplementary Fig. 3C-D), and the Cpx-poor harzburgite vary gradually into Cpx-rich harzburgites and Cpx-poor lherzolites (grouped as Cpx-rich harzburgites in this study)[12,49,51] (Fig. 3). Clinopyroxene grains in the Cpx-rich harzburgites show extended growth into the interstitial spaces and are characterized by prevalent figure-like protrusions, forming clinopyroxenite veins at times[40,51] (Fig. 3). The compositions of both chromite and clinopyroxene grains in the harzburgites vary from those with MORB-like at the bottom to more boninitic-like affinities at the top of the mantle sequence[12,49,51] (Fig. 3). The MTZ is mainly made up of dunites[40,52]

(Fig. 2D and 3), and the chromite deposits are all distributed along the mantle-MTZ boundary[12,49,52] (Fig. 2D and 3). Apart from some high-Al chromitites[12] (Sampling location 5 in Fig. 2D), the majority of chromitites in the block belong to the high-Cr variety and are everywhere spatially associated with dunites (Fig. 3; Supplementary Fig. 3E-G). The MTZ dunites vary stratigraphically upward into layered wehrlites and pyroxenites near the MTZ-crust boundary (Fig. 3; Supplementary Fig. 3H). The lithological distribution, petrographic features and chemical variations above have been ascribed to the combined effects of an early event of refertilization by asthenospheric components and later modification of the refertilized peridotites by Mg-rich melts related to different types of chromite mineralization[12,51]. The former event took place in the whole mantle sequence and converted all peridotites to Cpx-rich harzburgites, whereas the latter happened only at the uppermost mantle sequence, consuming pyroxene in the previously refertilized mantle and resulting in Cpx-poor harzburgites, dunites and chromitites under varying melt/rock ratios in both the upper mantle and MTZ[51].

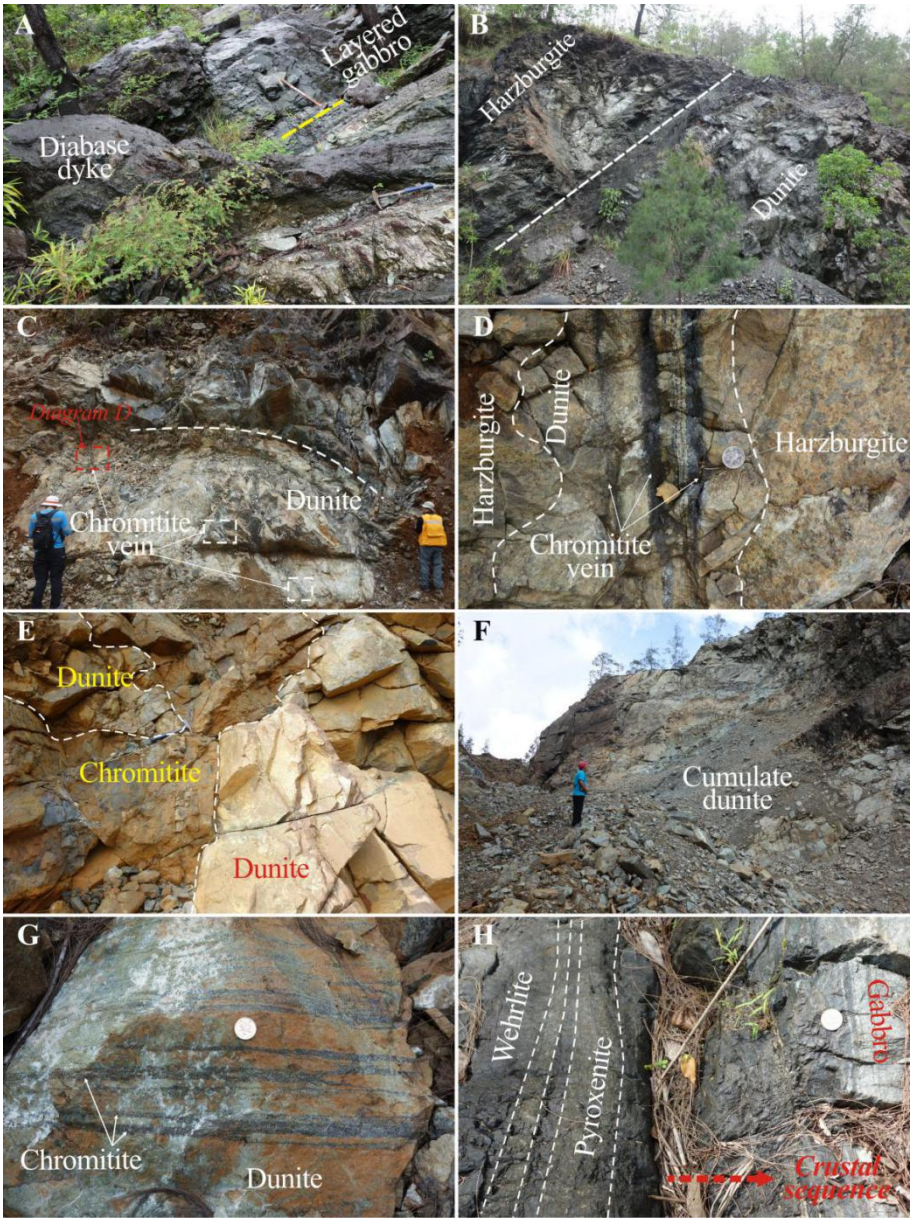

Supplementary Fig-3. Outcrops of different lithologies and their spatial relationship in the Coto (A-B) and Acoje blocks (C-H). (A): Layered gabbro and diabase dyke at the lowermost crustal sequence of the Coto block. The yellow mark the occurrence of the gabbro layer. (B): Harzburgite and dunite at the uppermost mantle sequence of the Coto block. (C): Contact between harzburgite and dunite bodies at top of the Acoje mantle sequence (near the Stop-4 in Fig.2D). Chromitite veins (~ 3-10 cm wide) can be found in the dunite body. (D): Close-up image showing detailed spatial relationships among chromitite vein, dunite and harzburgite (country rock) at top of the Acoje mantle sequence (near the Stop-6 in Fig.2D). The zones of chromitite and dunite were reaction products between the harzburgite and parental magmas of the chromitites. (E): Co-existing chromitite and dunite bodies (Stop-7 in Fig.2D). (F): Dunite body of cumulative origin in the Acoje MTZ (Near the Stop-6 in Fig.2C). (G): Interlayered dunite and chromitite found in the dunite body showed the panel F, supporting their cumulative origin. (H): Layered wehrlites, pyroxene and gabbros at the topmost part of the MTZ. Presence of gabbros marks the bottom level of the Acoje crustal sequence.

Supplementary Note-2: Fractional melting model and related parameters used in the Fig. 4D.

The TiO_2 content of fertile MORB mantle (FMM) used for the modeling is set to be 0.18% according to Pearce et al. show[53]. The modes (X_i) of olivine, orthopyroxene, clinopyroxene and spinel grains in the FMM are set to be 58.9%, 23.5%, 14.7% and 2.80%, respectively, as were used in Jerram et al. show[54] for fertile spinel peridotites. The melting modes (p_i) of olivine, orthopyroxene, clinopyroxene and spinel used in the forward modeling are set to be −0.29%, 0.46%, 0.71% and 0.11% under anhydrous conditions according to Jerram et al. show[54]. The values are set as −0.205%, 0.505%, 0.63% and 0.07% under hydrous conditions by averaging relevant data compiled in Gaetane & Grove show[55]. Melting of the FMM is supposed to happen under anhydrous condition, whereas melting of the mantle residues (MR) after 10%, 15% and 20% melting degrees are supposed to happen under hydrous conditions. The partition coefficients (k) of Ti between melt and olivine, orthopyroxene, clinopyroxene and spinel are 0.015, 0.15, 0.3 and 0.07, respectively, according to Kelemen et al. show[56].

The melting equations for obtaining the TiO_2 contents of melts (Cl) and solid residues (Cs) during fractional melting are listed as below:

$$Cl = (Co/F)*[1 - (1 - PF/Do)(1/P)]$$

$$Cs = [Co /(1-F)]*[(1 - PF/Do)(1/P)]$$

$$Do = Xo(ol)*k(ol) + Xo(opx)*k(opx) + Xo(cpx)*k(cpx) + Xo(sp)*k(sp)$$

$$P = p(ol)*k(ol) + p(opx)*k(opx) + p(cpx)*k(cpx) + p(sp)*k(sp)$$

Where Co, Xo, Do, F and P represent the Ti contents in the starting peridotites (not necessarily FMM), the mode of each phase in the starting peridotites, initial bulk-rock distribution coefficients of Ti, partial melting degree, and bulk reaction coefficient of Ti, respectively. When some a phase is used out during the calculation, the overall modes of all phase will be re-normalized to 100% for further processing.

Supplementary Table-1 Major element compositions of chromite in chromitites and Re-Os concentrations and isotopes of chromitites and harzburgites.

Sample	GPS Coordinates and Location	Cr#	TiO_2 (wt.%)	Re(ppb)	2SE	Os (ppb)	2SE	$^{187}Os/^{188}Os$	2SE	$^{187}Re/^{188}Os$	2SE
Acoje chromitites											
AC-01*	15°43'13"N, 120°03'22"E; Stop-7	73.4	0.21	0.118	0.028	64.828	0.126	0.12734	0.00015	0.036	0.003
AC-05*	15°43'13"N, 120°03'22"E; Stop-7	71.9	0.18	0.486	0.043	24.588	0.028	0.12700	0.00024	0.095	0.008
AC-19	15°43'13"N, 120°03'22"E; Stop-7	74.8	0.21	0.063	0.038	12.707	0.014	0.12683	0.00022	0.024	0.014
AC-38	15°43'13"N, 120°03'22"E; Stop-7	74.8	0.19	0.073	0.026	32.955	0.073	0.12844	0.00016	0.011	0.004
AC-33	15°43'13"N, 120°03'22"E; Stop-7	74.0	0.19	0.099	0.027	36.781	0.118	0.12881	0.00021	0.013	0.004
AC-57	15°42'0.9"N, 120°03'23"E; Stop-6	73.2	0.19	0.036	0.027	135.165	1.084	0.12760	0.00024	0.001	0.001
AC-42	15°42'36"N, 120°03'21"E; Stop-5	46.2	0.15	0.052	0.027	1.659	0.001	0.13205	0.00047	0.151	0.078
AC-45	15°42'36"N, 120°03'21"E; Stop-5	46.8	0.15	0.071	0.050	1.862	0.001	0.14710	0.00045	0.185	0.131
AC-46	15°42'36"N, 120°03'21"E; Stop-5	46.6	0.15	0.063	0.025	4.778	0.004	0.13085	0.00038	0.063	0.026
Coto chromitites											
ZB-03*	120°05'33"E, 15°34'46"N; Open pit	48.3	0.22	0.301	0.009	12.245	0.029	0.12942	0.00022	0.118	0.004
ZB-07*	120°05'33"E, 15°34'46"N; Open pit	50.9	0.08	0.157	0.009	18.378	0.087	0.13294	0.00024	0.059	0.004
ZB-10*	120°05'33"E, 15°34'46"N; Open pit	42.7	0.14	0.120	0.008	10.239	0.165	0.12829	0.00052	0.057	0.004
ZB-12*	120°05'33"E, 15°34'46"N; Open pit	45.7	0.11	0.224	0.015	11.509	0.089	0.12888	0.00048	0.094	0.006
ZB-14*	120°05'33"E, 15°34'46"N; Open pit	41.9	0.18	0.067	0.007	1.949	0.005	0.13489	0.00036	0.166	0.018
C-26	120°05'0.5"E, 15°34'21"N; Open pit	47.3	0.06	0.101	0.006	26.158	0.216	0.12605	0.00027	0.019	0.001
C-31	120°05'0.5"E, 15°34'21"N; Open pit	46.6	0.07	0.073	0.006	13.153	0.043	0.12971	0.00021	0.027	0.002
DEC-01	120°05'0.5"E, 15°34'21"N; Open pit	47.3	0.03	0.104	0.008	10.007	0.037	0.12904	0.00028	0.050	0.004
DEC-02	120°05'0.5"E, 15°34'21"N; Open pit	47.2	0.05	0.098	0.008	14.497	0.046	0.12869	0.00025	0.032	0.003

Note: the Cr# and TiO_2 contents of chromite in the chromitites with and without * are from Zhou et al. show[14] and Zhang et al. show[8,12], respectively.

Supplementary Table-1 Continued

Sample	GPS Coordinates and Location	Re (ppb)	2SE	Os (ppb)	2SE	$^{187}Os/^{188}Os$	2SE	$^{187}Re/^{188}Os$	2SE
Cpx-rich harzburgites									
A-75	15°41'49"N, 120°02'58"E; Stop-4	0.172	0.012	2.843	0.016	0.12736	0.00017	0.045	0.009
A-78	15°41'49"N, 120°02'58"E; Stop-4	0.290	0.012	3.456	0.015	0.12654	0.00021	0.404	0.016
A-154	15°41’31”N, 120°02’44”E; Stop-3	0.173	0.008	5.325	0.064	0.12599	0.00020	0.156	0.007
Cpx-poor harzburgites									
C-14	15°34'20"N, 120°05'50"E; Open pit	0.081	0.002	2.491	0.016	0.12600	0.00025	0.156	0.005
C-15	15°34'20"N, 120°05'50"E; Open pit	0.027	0.005	4.426	0.039	0.12647	0.00016	0.029	0.006
C-20	15°34'20"N, 120°05'50"E; Open pit	0.063	0.005	1.848	0.011	0.12338	0.00020	0.165	0.013
C-21	15°34'20"N, 120°05'50"E; Open pit	0.149	0.009	5.275	0.039	0.12391	0.00022	0.136	0.008
C-22	15°34'20"N, 120°05'50"E; Open pit	0.063	0.013	3.292	0.014	0.12428	0.00014	0.039	0.007
A-120	15°42’36”N, 120°03’21”E; Stop-5	0.442	0.013	7.866	0.120	0.12846	0.00022	0.271	0.009
A-124	15°42’36”N, 120°03’21”E; Stop-5	0.108	0.005	3.733	0.035	0.12532	0.00016	0.139	0.006
(BIR-1)-01		0.683	0.012	0.342	0.000	0.13419	0.00025	9.628	0.166
(BIR-1)-02		0.693	0.013	0.332	0.001	0.13406	0.00023	10.063	0.185
(BIR-1)-03		0.684	0.011	0.352	0.000	0.13403	0.00022	9.357	0.146
BLK-01		0.9	1.2	1.083	0.020	0.15155	0.00324		
BLK-02		0.8	1.2	0.908	0.046	0.16892	0.00218		
BLK-03		1.7	0.9	0.362	0.010	0.19252	0.00210		

Supplementary References

1. Matsumoto, I., Arai, S. & Yamauchi, H. High-Al podiform chromitites in dunite-harzburgite complexes of the Sangun zone, central Chugoku district, Southwest Japan. J. Asian Earth Sci. **15**, 295-302 (1997).
2. Arai S. & Yurimoto H. Podiform chromitites of the Tari-Misaka ultramafic complex, southwestern Japan, as mantle-melt interaction products. Econ. Geol. **89**, 1279-1288 (1994).
3. Zhou, M.F. et al. Melt/mantle interaction and melt evolution in the Sartohay high-Al chromite deposits of the Dalabute ophiolite (NW China). J. Asian Earth Sci. **19**, 517-534 (2001).
4. Robinson, P.T., Zhou, M.F., Hu, X.F., Reynolds, P., Wenji, B. & Yang, J. Geochemical constraints on the origin of the Hegenshan Ophiolite, Inner Mongolia, China. J. Asian Earth Sci. **17**, 423-442 (1999).
5. Proenza, J., Gervilla, F., Melgarejo, J. & Bodinier, J.L. Al-and Cr-rich chromitites from the Mayari-Baracoa ophiolitic belt (eastern Cuba); consequence of interaction between volatile-rich melts and peridotites in suprasubduction mantle. Econ. Geol. **94**, 547-566 (1999).
6. Marchesi, C., Garrido, C.J., Godard, M., Proenza, J.A., Gervilla, F. & Blanco-Moreno, J. Petrogenesis of highly depleted peridotites and gabbroic rocks from the Mayarí-Baracoa Ophiolitic Belt (eastern Cuba). Contrib. Mineral. Petr. **151**, 717-736 (2006).
7. Rui, H.C., Yang, J.S., Castro, A.I.L., Zheng, J.P., Lian, D.Y., Wu, W.W. & Marino, Y.V. Ti-poor high-Al chromitites of the Moa-Baracoa ophiolitic massif (eastern Cuba) formed in a nascent forearc mantle. Ore Geol. Rev. **144**, 104847 (2022).
8. Zhang, P.F. et al. Sluggish slab rollback at the early stage of flux melting during subduction initiation: Li isotopic evidence from the Coto high-Al chromite deposit, Zambales ophiolite, Philippines. J. Geophys. Res.-Sol. Ea. **128**, e2022JB025562 (2023).
9. Yumul Jr, G.P. & Dimalanta, C.B. Geology of the Southern Zambales Ophiolite Complex,(Philippines): juxtaposed terranes of diverse origin. J. Asian Earth Sci. **15**, 413-421 (1997).
10. Hernández-González, J.S. et al. Petrology and geochemistry of high-Al chromitites from the Medellín Metaharzburgitic Unit (MMU), Colombia. Bol. Soc. Geol. Mex. **72**, DOI: 10.18268/BSGM2020v72n3a120620 (2020).
11. Liipo, J., Vuollo, J., Nykänen, V., Piirainen, T., Pekkarinen, L. & Tuokko, I. Chromites from the early Proterozoic Outokumpu-Jormua ophiolite belt: a comparison with chromites from Mesozoic ophiolites. Lithos **36**, 15-27 (1995).
12. Zhang, P.F., Zhou, M.F. & Yumul Jr, G.P. Coexistence of high-Al and high-Cr chromite orebodies in the Acoje block of the Zambales ophiolite, Philippines: Evidence for subduction initiation. Ore Geol. Rev. **126**, 103739 (2020).
13. Greenbaum, D. The chromitiferous rocks of the Troodos ophiolite complex, Cyprus. Econ. Geol. **72**, 1175-1194 (1977).

14. Batanova, V.G. & Sobolev, A.V. Compositional heterogeneity in subduction-related mantle peridotites, Troodos massif, Cyprus. Geology **28**, 55-58 (2000).
15. Zhang, P.F., Uysal, I., Zhou, M. F., Su, B.X. & Avcı, E. Subduction initiation for the formation of high-Cr chromitites in the Kop ophiolite, NE Turkey. Lithos **260**, 345-355 (2016).
16. Uysal, I., Tarkian, M., Sadiklar, M.B., Zaccarini, F., Meisel, T., Garuti, G. & Heidrich, S. Petrology of Al-and Cr-rich ophiolitic chromitites from the Muğla, SW Turkey: implications from composition of chromite, solid inclusions of platinum-group mineral, silicate, and base-metal mineral, and Os-isotope geochemistry. Contrib. Mineral. Petr. **158**, 659-674 (2009).
17. Uysal, İ. et al. Coexistence of abyssal and ultra-depleted SSZ type mantle peridotites in a Neo-Tethyan Ophiolite in SW Turkey: Constraints from mineral composition, whole-rock geochemistry (major–trace–REE–PGE), and Re–Os isotope systematics. Lithos, **132**, 50-69 (2012).
18. Xu, Y., Chen, S., Parlak, O., Arai, S., Dönmez, C. & Hong, J. Discovery of extremely high-Al podiform chromitites from the Lycian (Marmaris) ophiolite, SW Turkey: Implications for chromitite genesis. Ore Geol. Rev. **127**, 103817 (2020).
19. Takazawa, E., Okayasu, T. & Satoh, K. Geochemistry and origin of the basal lherzolites from the northern Oman ophiolite (northern Fizh block). Geochem. Geophy. Geosy. **4**. *https://doi.org/10.1029/2001GC000232* (2003).
20. Rollinson, H., Adetunji, J., Yousif, A.A. & Gismelseed, A.M. New Mössbauer measurements of $Fe^{3+}/\Sigma Fe$ in chromites from the mantle section of the Oman ophiolite: evidence for the oxidation of the sub-oceanic mantle. Mineral. Mag. **76**, 579-596 (2012).
21. Moutte, J. Chromite deposits of the Tiebaghi ultramafic massif, New Caledonia. Econ. Geol. 77, 576-591 (1982).
22. Ulrich, M., Picard, C., Guillot, S., Chauvel, C., Cluzel, D. & Meffre, S. Multiple melting stages and refertilization as indicators for ridge to subduction formation: The New Caledonia ophiolite. Lithos **115**, 223-236 (2010).
23. Melcher, F., Grum, W., Simon, G., Thalhammer, T.V. & Stumpfl, E.F. Petrogenesis of the ophiolitic giant chromite deposits of Kempirsai, Kazakhstan: a study of solid and fluid inclusions in chromite. J. Petrol. **38**, 1419-1458 (1997).
24. Savelieva, G.N., Batanova, V.G., Kuz'min, D.V. & Sobolev, A.V. Composition of minerals in mantle peridotites as proxy of ore-forming processes in the mantle: Evidence from ophiolites in the Voykar-Synya and Kempirsai Massifs. Lithol. Miner. Resour. **50**, 80-91 (2015).
25. Saveliev, D.E. & Fedoseev, V.B. Solid-state redistribution of mineral particles in the upwelling mantle flow as a mechanism of chromite concentration in the ophiolite ultramafic rocks (by the example of Kraka ophiolite, the Southern Urals). Georesources, **21**, 31-46 (2019).

26. Garuti, G., Pushkarev, E.V., Gottman, I.A. & Zaccarini, F. Chromite-PGM Mineralization in the Lherzolite Mantle Tectonite of the Kraka Ophiolite Complex (Southern Urals, Russia). Minerals **11**, 1287 (2021).
27. Gong, X.H. et al. Recycling of ancient subduction-modified mantle domains in the Purang ophiolite (southwestern Tibet). Lithos **262**,11-26 (2016).
28. Xiong, F., Yang, J., Xu, X., Kapsiotis, A., Hao, X. & Liu, Z. Compositional and isotopic heterogeneities in the Neo-Tethyan upper mantle recorded by coexisting Al-rich and Cr-rich chromitites in the Purang peridotite massif, SW Tibet (China). J. Asian Earth Sci. **159**, 109-129 (2018).
29. Xiong, F. et al. High-Al and high-Cr podiform chromitites from the western Yarlung-Zangbo suture zone, Tibet: implications from mineralogy and geochemistry of chromian spinel, and platinum-group elements. Ore Geol. Rev. **80**, 1020-1041 (2017).
30. Xiong, Q., Henry, H., Griffin, W.L., Zheng, J.P., Satsukawa, T., Pearson, N.J. & O'Reilly, S.Y. High-and low-Cr chromitite and dunite in a Tibetan ophiolite: evolution from mature subduction system to incipient forearc in the Neo-Tethyan Ocean. Contrib. Mineral. Petr. **172**, 1-22 (2017).
31. Zhang, P.F., Zhou, M.F., Malpas, J. & Robinson, P.T. Origin of high-Cr chromite deposits in nascent mantle wedges: petrological and geochemical constraints from the neo-Tethyan Luobusa ophiolite, Tibet. Ore Geol. Rev. **123**, 103581 (2020).
32. Zhou, M.F., Robinson, P.T., Su, B.X., Gao, J.F., Li, J.W., Yang, J.S. & Malpas, J. Compositions of chromite, associated minerals, and parental magmas of podiform chromite deposits: The role of slab contamination of asthenospheric melts in suprasubduction zone environments. Gondwana Res. **26**, 262-283 (2014).
33. Xiong, F., Zoheir, B., Robinson, P. T., Yang, J., Xu, X. & Meng, F. Genesis of the Ray-Iz chromitite, Polar Urals: Inferences to mantle conditions and recycling processes. Lithos, **374**, 105699 (2020).
34. Liu, X. et al. Initial subduction of Neo-Tethyan ocean: Geochemical records in chromite and mineral inclusions in the Pozantı-Karsantı ophiolite, southern Turkey. Ore Geol. Rev. 110, 102926 (2019).
35. Su, B. et al. Distinctive melt activity and chromite mineralization in Luobusa and Purang ophiolites, southern Tibet: constraints from trace element compositions of chromite and olivine. Sci. Bull. **64**, 108-121 (2019).
36. Gervilla, F., et al. Distribution of platinum-group elements and Os isotopes in chromite ores from Mayarí-Baracoa Ophiolitic Belt (eastern Cuba). Contrib. Mineral. Petr. **150**, 589-607 (2005).
37. Xiong, F.H. et al. Different type of chromitite and genetic model from Luobusa ophiolite Tibet. Acta Petrol. Sin. **30**, 2173-2163 (2014).
38. Xiong, Q. et al. Sulfide in dunite channels reflects long-distance reactive migration of mid-ocean-ridge melts from mantle source to crust: a Re-Os isotopic perspective. Earth Planet Sc. Lett. 531, 115969 (2020).

39. Hawkins, J.W. & Evans, C.A. Geology of the Zambales Range, Luzon, Philippine Islands: Ophiolite derived from an island arc-back arc basin pair. Geophys. Monogr. Ser. **27**, 95-123 (1983).
40. Leblanc, M. & Violette, J.F. Distribution of aluminum-rich and chromium-rich chromite pods in ophiolite peridotites. Econ. Geol. **78**, 293-301 (1983).
41. Hock, M. & Friedrich, G. Structural features of ophiolitic chromitites in the Zambales Range, Luzon, Philippines. Miner. Deposita **20**, 290-301 (1985).
42. Xiong, F.H., Yang, J.S. & Liu, Z. Multi-stage formation of the podiform chromitite. Geol. China, **40**, 820-839 (2013).
43. Geary, E.E., Kay, R.W., Reynolds, J.C. & Kay, S.M. Geochemistry of mafic rocks from the Coto Block, Zambales ophiolite, Philippines: trace element evidence for two stages of crustal growth. Tectonophysics, **168**, 43-63 (1989).
44. Encarnación, J.P., Mukasa, S.B. & Obille Jr, E.C. Zircon U-Pb geochronology of the Zambales and Angat Ophiolites, Luzon, Philippines: Evidence for an Eocene arc-back arc pair. J. Geophys. Res.-Sol. Ea. **98**, 19991-20004 (1993).
45. Perez, A., Umino, S., Yumul Jr, G.P. & Ishizuka, O. Boninite and boninite-series volcanics in northern Zambales ophiolite: doubly vergent subduction initiation along Philippine Sea plate margins. Solid Earth, **9**, 713-733 (2018).
46. Evans, C.A., Casteneda, G. & Franco, H. Geochemical complexities preserved in the volcanic rocks of the Zambales ophiolite, Philippines. J. Geophys. Res.-Sol. Ea. **96**, 16251-16262 (1991).
47. Yumul, Jr, G.P. Varying mantle sources of supra-subduction zone ophiolites: REE evidence from the Zambales Ophiolite Complex, Luzon, Philippines. Tectonophysics **262**, 243-262 (1996).
48. Yumul Jr, G.P., Dimalanta, C.B., Faustino, D.V. & De Jesus, J.V. Translation and docking of an arc terrane: geological and geochemical evidence from the southern Zambales Ophiolite Complex, Philippines. Tectonophysics **293**, 255-272 (1998).
49. Evans, C. & Hawkins Jr, J.W. Compositional heterogeneities in upper mantle peridotites from the Zambales Range Ophiolite, Luzon, Philippines. Tectonophysics, **168**, 23-41 (1989).
50. Yumul, G.P. Zambales Ophiolite Complex (Philippines) transition-zone dunites: restite, cumulate, or replacive products? Int. Geol. Rev. **46**, 259-272 (2004).
51. Zhang, P.F., Zhou, M.F., Yumul Jr, G.P. & Wang, C.Y. Geodynamic setting of high-Cr chromite mineralization in nascent subduction zones: Li isotopic and REE constraints from the Zambales ophiolite, Philippines. Lithos **384**, 105975 (2021).
52. Yumul Jr, G.P. The Acoje block platiniferous dunite horizon, Zambales ophiolite complex, Philippines: melt type and associated geochemical controls. Resour. Geol. **51**, 165-174 (2001).
53. Pearce, J.A., Barker, P.F., Edwards, S.J., Parkinson, I.J. & Leat, P.T. Geochemistry and tectonic significance of peridotites from the South Sandwich arc–basin system, South Atlantic. Contrib. Mineral. Petr. **139**, 36-53 (2000).

54. Jerram, M., Bonnand, P., Harvey, J., Ionov, D. & Halliday, A.N. Stable chromium isotopic variations in peridotite mantle xenoliths: Metasomatism versus partial melting. Geochim. Cosmochim. Acta **317**, 138-154 (2022).
55. Gaetani, G.A. & Grove, T.L. The influence of water on melting of mantle peridotite. Contributions to Mineralogy and Petrology **131**, 323-346 (1998).
56. Kelemen, P.B., Johnson, K.T.M., Kinzler, R.J. & Irving, A.J. High-field-strength element depletions in arc basalts due to mantle–magma interaction. Nature **345**, 521-524 (1990).